Transitions from α to π Helix Observed in Molecular Dynamics Simulations of Synthetic Peptides†

Kyung-Hoon Lee, David R. Benson, and Krzysztof Kuczera*

Department of Chemistry, University of Kansas, 2010 Malott Hall, Lawrence, Kansas 66045

Received May 17, 2000; Revised Manuscript Received August 2, 2000

ABSTRACT: Molecular dynamics simulations were carried out for three 13-residue peptides of the form AcNH-A-A-E-X-A-E-A-H-A-A-E-K-A-$CONH_2$ with X = A, F, and W. All three peptides exhibited unexpected dynamical behavior, undergoing a transition from an α-helical to a π-helical structure in the course of 5-ns trajectories in aqueous solution. Analysis of peptide length, accessible surface, interaction energies, hydrogen bonding, and dihedral angles was consistent with α → π transitions at 2800, 500, and 800 ps for X = A, F and W, respectively. The transitions occurred sequentially and cooperatively, propagating from the C- to the N-terminus for X = A and W and from the center toward both termini for X = F. The time scale of the overall transition ranged from 300 to 500 ps. For all three peptides the backbone structural transition was accompanied by a concerted rearrangement of the charged side chains, including a 3 Å increase in the distance between carboxylate groups of Glu-3 and Glu-6. During the transition the peptide backbone hydrogen-bonding patterns were disrupted at the interface between the α-helical and nascent π-helical regions, with peptide groups forming water-bridged hydrogen bonds. The peptide structures exhibited significant fluidity, with individual residues sampling α-, π-, and 3_{10}-helical conformations, as well as a "coil" state, without any intramolecular hydrogen bonds. The studied peptides have been designed to form α-helices when incorporated in novel hemoprotein model compounds, peptide-sandwiched mesohemes, which consist of two identical peptides covalently attached to an Fe(III) mesoporphyrin [Liu, D., Williamson, D. A., Kennedy, M. L., Williams, T. D., Morton, M. M., and Benson, D. R. (1999) *J. Am. Chem. Soc. 121,* 11798−11812]. The possibility of adopting π-helical structures by the constituent peptides may influence the properties of the hemoprotein models.

Helices are predominant secondary structure elements of proteins. The helical structures are stabilized by intramolecular hydrogen bonds between a C═O oxygen and an N−H hydrogen. The helical types (x_y) are defined by the number of the residues (x) and the number of atoms per single turn (y). α-Helical (3.6_{13}) and γ-helical (5.1_{17}) structures were first hypothesized by Pauling and Corey (*1*). Subsequently, Donohue (*2*) considered the possibility of additional structures: 2.2_7, 3_{10}, 4.3_{14}, and 4.4_{16} (π) helices. Low and Baybutt (*3*) also postulated the possibility of π-helices. The various helix forms differ in their hydrogen-bonding patterns. In α-helices the peptide C═O of residue i forms a hydrogen bond with the peptide N−H of residue $i + 4$ ($i\cdots i + 4$ pattern); the patterns are $i\cdots i + 3$ for 3_{10} helices and $i\cdots i + 5$ for π-helices. The existence of the α- and 3_{10}-helices is currently well-established. In protein crystals, ca. 31% of amino acid residues are in α-helical structures, while 3−4% are in 3_{10} helices (*4*−*6*). Also, peptides adopting the α-helical (*7*−*9*) and 3_{10}-helical (*10, 11*) forms are known. 3_{10}-Helices often occur at C- or N-termini of α-helices in proteins (*6*). They are also the preferred structure for short α-methylated peptides (*9, 10*). On the other hand, occurrences of π-helices appear to be quite rare. Several reasons for the apparent lack of stability of the π-helix have been put forward: backbone dihedral angles in a less favorable conformational region than the α-helix (*12, 13*), the existence of a 1 Å hole in the center of the helix, which is sufficiently wide to cause loss of van der Waals interactions but not wide enough to accommodate a water molecule (*3*), and the large entropic cost of initiating a π-helix, in which five residues have to be preorganized before the first helical hydrogen bond is formed (*13, 14*).

There is limited experimental evidence for the existence of π-helical structures in peptides and proteins (*15*). A recent review identified about 10 protein structures in which π-helical turns occur, including fumarase C (*15, 16*), glycogen phosphorylase *b* (*15*), lipoxygenase (*17, 18*), and nitrogenase (*15*). Most of the π-helices found in the protein structures are involved in the formation and function of specific binding sites (*15*). The existence of a left-handed π-helical structure was inferred from infrared spectra of thin films of poly(β-phenethyl L-aspartate) (*19*). It has also been proposed that peptides in hydrophobic environments, such as lipid vesicles or membranes, might form π-helical structures (*20*).

Interestingly, the presence of the π-helix has been found in several recent molecular dynamics (MD) simulations. In simulations of a fragment of pulmonary surfactant lipoprotein SP-C in water, eight consecutive residues adopted the

† Supported in part by the Petroleum Research Fund of the American Chemical Society (Grant 33126-AC4 to K.K.) and by the National Institutes of Health (Grant R29-GM52431 to D.R.B.).

* Address correspondence to this author: fax (785) 864-5396; phone (785) 864-5060; e-mail kkuczera@ukans.edu.

10.1021/bi001126b CCC: $19.00
Published on Web 10/21/2000

π-helical conformation (*21*). In blocked peptides of the form Amn-$(AAXAA)_3$-Cbx (where Amn is $COCH_3$ and Cbx is $NHCH_3$), several residues populated states with both α and π-helical hydrogen-bonding patterns during the simulation in aqueous solution (*22*); the stabilization of the $i\cdots i+5$ hydrogen bonds was attributed to water-bridged side chain−side chain interactions. Several occurrences of π-helical and other nonstandard hydrogen bonds were seen in simulations of alamethicin (*23*). For the 29-residue membrane spanning fragment of the ErbB-2 receptor, transitions from the initial α-helix to mainly π-helical structures were observed in MD simulations in vacuum and in a solvated lipid bilayer environment (*24*). In this case the stabilization of the π-helix was attributed to a high content of bulky Val side chains.

Our group has undertaken studies of ideal decaalanine helices, which have identical conformations at each residue and can thus be characterized by the two conformational parameters (φ, ψ) (*25*, *26*). We have found that both the α- and π-helices correspond to local minima on the decaalanine conformational free energy surface. While the π-helix was much less stable than the α-helix in a vacuum (*26*), the two structures had comparable stabilities in water and DMSO solution (Mahadevan et al., unpublished results). The α-helical free energy minimum in solution was found at (φ, ψ) = (−64°, −42°), close to the (−62°, −41°) average geometry found in α-helices for protein crystals (*5*). On the other hand, our decaalanine π-helical free energy minimum was located at (−75°, −56°) in aqueous solution and at (−77°, −54°) in vacuum (*26*), which is significantly different from the proposed model values of (−57°, −70°) (*4*, *13*). Our conformational free energy surfaces were quite flat for anticorrelated variation of φ and ψ, which structurally led to changes in helix radius while leaving the hydrogen-bonding pattern unchanged. Thus helical structures obtained under different conditions (solvent, substitution at C_α) tended to fall along antidiagonal straight lines: $\varphi + \psi \approx -107°$ for α-helices and $\varphi + \psi \approx -131°$ for π-helices. The model π-helix geometry of (φ, ψ) = (−57°, −70°) lies close to this last line. Our π-helical free energy minimum structure at (−75°, −56°), which has not previously been considered, has a number of advantageous properties. It has a volume that is almost identical to and a surface area that is about 5% smaller than the α-helix, and it has strong favorable interactions with solvent (Mahadevan et al., unpublished results). We have analyzed the conformations of residues *i* involved in the $i\cdots i+5$ hydrogen bonds in the set of protein structures described by Weaver (*15*). After eliminating several cases with positive φ or ψ, which do not fall into the left-handed helix region of the Ramachandran plot, we found φ values ranging from −115° to −62° and ψ from −73° to −21°, with the average falling at (φ, ψ) = (−74°, −51°). This average is in quite good agreement with the calculated (−75°, −56°) free energy minimum in water.

In this work, we present results of simulations for solvated peptides of the forms [AcNH-A-A-E-X-A-E-A-H-A-A-E-K-A-$CONH_2$, with X = A, F, and W], which display unexpected dynamical behavior. During 5-ns MD trajectories in aqueous solution starting from α-helical structures, all three peptides undergo transitions to π-helices. The peptides under investigation attracted our interest because they are components of novel hemoprotein model compounds, peptide-sandwiched mesohemes (PSMs) (*27*, *28*). The PSMs consist of two identical 13-residue peptides covalently attached to Fe(III) mesoporphyrin II (*27*) or Fe(III) mesoporphyrin IX (*28*) via amide linkages between the porphyrin propionate groups and the ϵ-amine group of lysine side chains. A histidine (His) residue in each peptide coordinates to the iron, inducing helical conformations in the peptides as determined by circular dichroism (CD) spectroscopy and ^{1}H NMR. The helix content in the PSM constructed from peptide 1 is ∼ 50% (*28*). Helicity is increased to ∼83% in the PSM constructed from peptide 3, due to favorable interactions between the tryptophan side chain and the porphyrin (*28*). The monomeric peptides exhibit CD spectra consistent with random coil conformations (*27*; Benson et al., unpublished experiments), a conclusion that is supported by temperature independence of the CD spectra (Benson et al., unpublished experiments). As a preliminary step to understanding the PSM systems, we have undertaken MD simulations of the peptides themselves. The goal was to obtain information on the structure and flexibility of the isolated peptides in solution. Comparison with simulation results of the full PSM systems could then be used to assess the influence on peptide structure and flexibility of the constraints due to nonbonded interactions and covalent links with the porphyrin. We describe here the details of the simulations of the individual peptides in aqueous solution in which the α- to π-helix structural transitions were serendipitously discovered.

MATERIALS AND METHODS

The CHARMM program (version 25) (*29*) and CHARMM version 22 all-atom protein topology and parameters (*30*) were used in all the calculations. The three 13-residue peptides were constructed in α-helical conformations with $\varphi = -57°$ and $\psi = -47°$. Each peptide was acetylated at the N-terminus and amidated at the C-terminus, and the side chains were in extended conformations. The peptides were immersed in a truncated octahedral water box constructed by cutting off corners from a cube of sides 46.35 Å. The TIP3P model of water was used (*31*). After water molecules overlapping with the peptides were deleted, 1662, 1658, and 1655 water molecules were left in the solvent box for simulations of peptides 1, 2 and 3, respectively. Initially the solvent was equilibrated with fixed positions of the solutes over 50 ps, followed by a 50 ps equilibration of the whole system. Finally, 5-ns MD trajectories were generated for each of the three peptides.

An atom-based 12.0 Å nonbonded cutoff distance was employed in all energy evaluations. A switching function between 10 and 12 Å and a shift function at 12.0 Å were applied for van der Waals and for electrostatics, respectively, to eliminate discontinuities due to the cutoff (*29*). Equilibration and trajectory generation were carried out by molecular dynamics simulations at constant pressure of 1 atm and temperature of 300 K, with periodic boundary conditions, by use of the Leapfrog integrator with a 2-fs time step. SHAKE constraints were applied to all the bonds involving hydrogen atoms (*32*). The Langevin piston method was used for constant pressure simulations (*33*) and the Hoover method

[1] Abbreviations: CD, circular dichroism; MD, molecular dynamics; PSMs, peptide-sandwiched mesohemes; rms, root-mean-square.

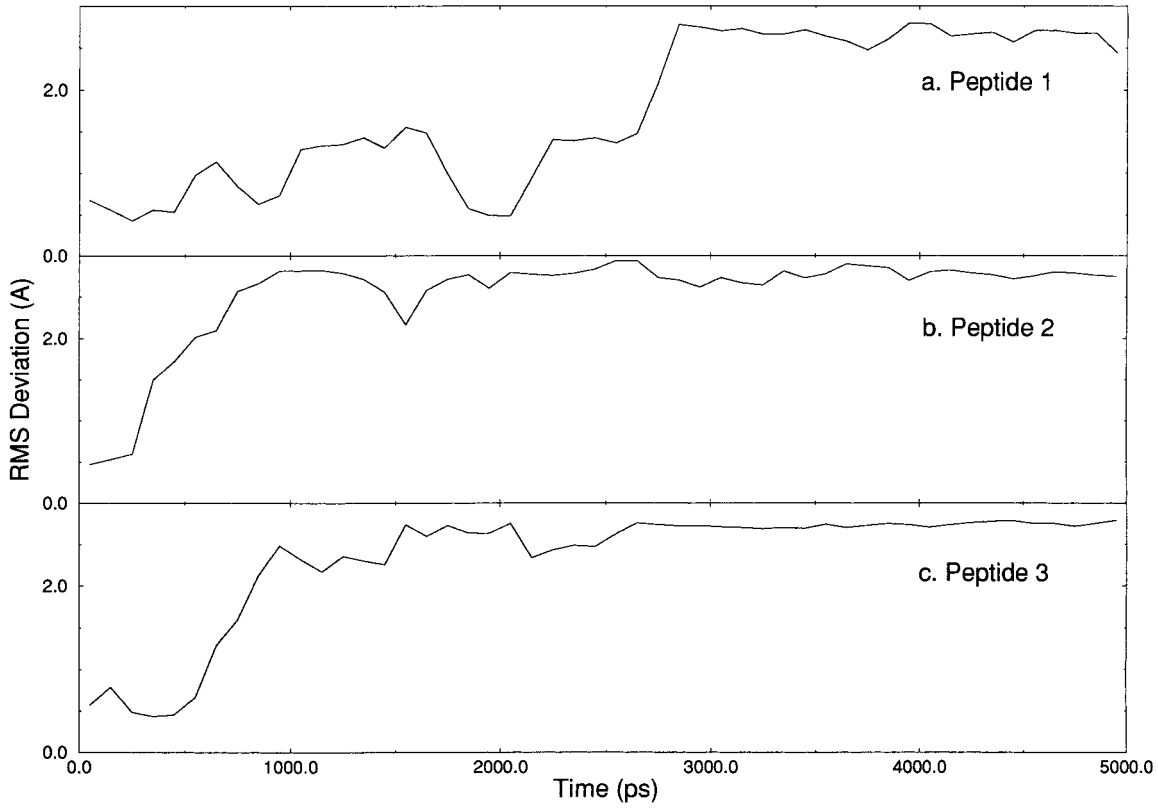

FIGURE 1: Time series of backbone root-mean-square deviations (in angstroms) from the starting structures of (a) peptide 1 (X = A), (b) peptide 2 (X = F), and (c) peptide 3 (X = W).

for constant temperature simulations (*34*). Coordinates were saved every 250 steps to produce trajectory files containing 10000 configurations for each 5-ns peptide simulation.

Solvent-accessible surface areas of the peptides were calculated for a probe of 1.6 Å radius by using the algorithm of Lee and Richards (*35*). Time series of all the backbone angles (φ and ψ) were calculated. Additional dihedrals φ-1 and ψ-13 were introduced to describe the conformations of the N-terminal acetyl and the C-terminal amide group, respectively. End-to-end distances of the peptides were calculated as the distances between C_α of Ala-1 (first residue) and C_α of Ala-13 (last residue).

Time series of $r_{i3}(t)$, $r_{i4}(t)$, and $r_{i5}(t)$ of distances between the C═O oxygen of residue i and N−H nitrogen of residues $i + 3$, $i + 4$, and $i + 5$ were calculated. The hydrogen bond (H-bond) type of residue i at time t was set to the type of contact with the shortest distance of the three $r_{min} = \min[r_{i3}(t), r_{i4}(t), r_{i5}(t)]$, if r_{min} was less than 4 Å. Otherwise, the residue was assigned to a "coil" state. Hydrogen-bond types of individual residues (from first to tenth) were assigned in this way. The hydrogen-bond types of the last three residues were not included in this analysis because they lack appropriate H-bond partners. After the H-bond types of all the individual residues were assigned, aggregate populations of each state were added up at each time step for the entire peptides. The populations of 3_{10}-helix, α-helix, π-helix, and coil states at each time step were then plotted.

In energy component analysis the CHARMM BLOCK facility was used (*36*) to divide the system into three parts: solvent, backbone, and side chains. The backbone was defined as the N, C_α, C, and O atoms of each peptide plus the hydrogens attached to these atoms and all atoms used in N- and C-terminal capping. The remaining peptide atoms were assigned to the side chains. With this partition, the backbone−backbone energy was defined as the sum of all internal strain (bond stretching, angle bending, Urey−Bradley, dihedral, and improper deformation) and nonbonded (van der Waals and electrostatics) terms involving atoms of the backbone only. Analogously, the side chain−side chain energy involved all internal strain and nonbonded terms involving side chain atoms only, while the backbone−side chain energy included all the mixed terms, involving atoms of both backbone and side chains. The solvation energy terms, backbone−solvent and side chain−solvent, involved all nonbonded interactions between the selected subset of solute atoms and the solvent (including solvent periodic images).

In the time series analysis, averages and standard deviations of the data were calculated. For some of the quantities, such as end-to-end distances, surface area, and interaction energies, we have also calculated the standard deviation of the mean to better estimate the uncertainty of the average values. The standard deviation of the mean was taken to be the standard deviation of the sample formed by subaverages of the data over 20 consecutive blocks of 500 points each.

The simulations were performed on the 16-processor SGI ORIGIN 2000 computer system at the Center for Advanced Scientific Computing at the University of Kansas and on a dual processor SGI OCTANE workstation. A 1-ns simulation of a solvated peptide system took about 390 h of CPU time on a single 195 MHz R10000 processor on either of these machines.

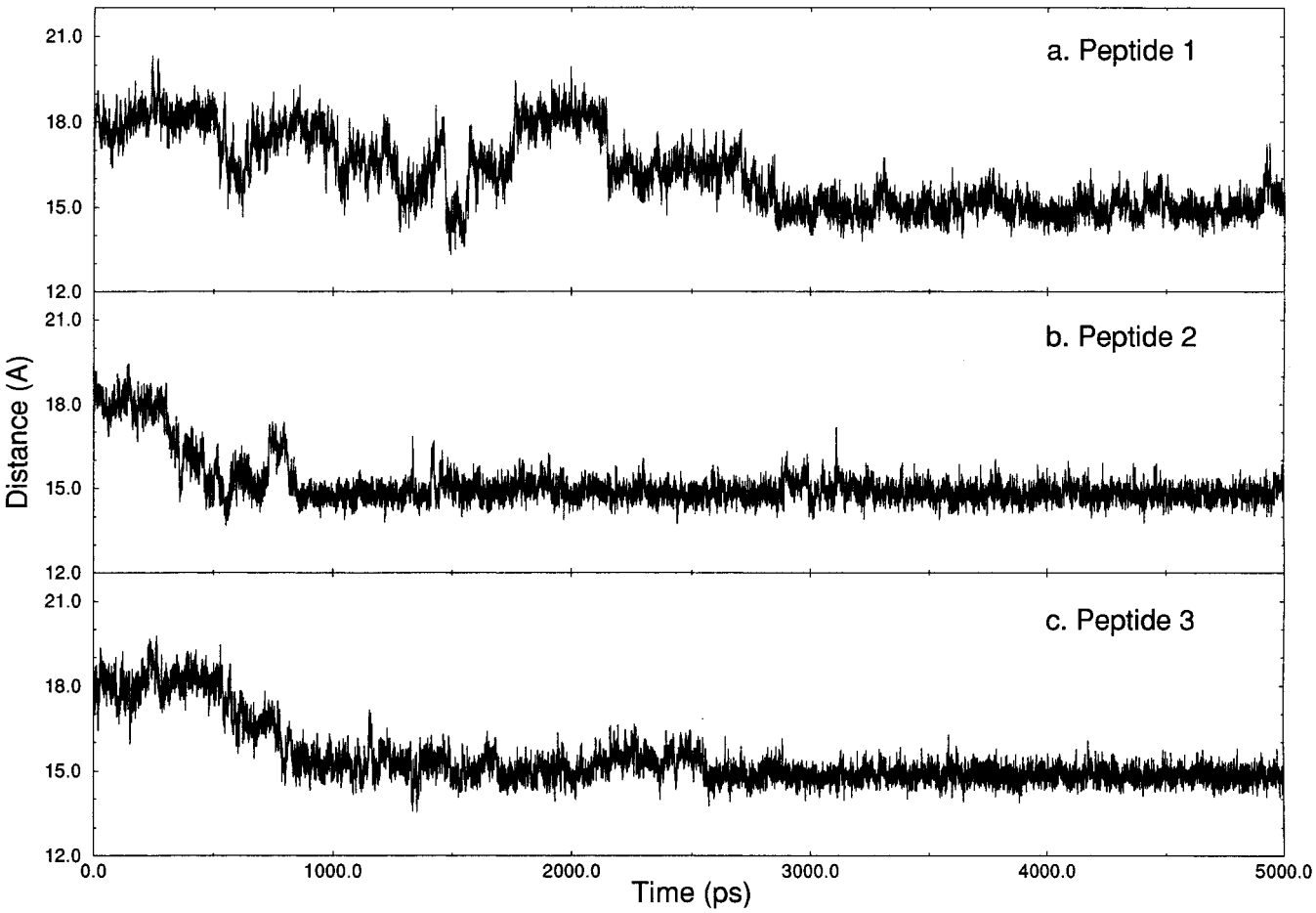

FIGURE 2: Time series of distance (in angstroms) between C_α of Ala-1 and C_α of Ala-13 of (a) peptide 1 (X = A), (b) peptide 2 (X = F), and (c) peptide 3 (X = W).

Table 1: Root Mean Square Deviations of Peptide Backbone from Starting Structure for First 100 ps and for Last 100 ps of MD Trajectories of Peptides 1, 2, and 3

peptide	0−100 ps	4900−5000 ps
1	0.6	2.4
2	1.5	2.7
3	0.9	2.8

RESULTS AND DISCUSSION

The analysis of the structure and dynamics of the three peptides examined in MD simulations is presented below. As described in the Materials and Methods section, a number of properties were calculated, all consistently indicating that each peptide undergoes a transition from an α-helical to a π-helical conformation.

General Description of Conformational Transition. The time evolutions of the backbone rms deviation of peptide trajectory structures from the starting conformation are shown in Figure 1. These data clearly indicate that a structural transition occurs in each of the simulations: in the 2600−2800 ps interval for peptide 1, 400−600 ps for peptide 2, and 700−900 ps for peptide 3. In all three cases the rms deviation remains close to 3 Å in the final part of the trajectories (Table 1). The peptide end-to-end distances, measured by the distance between the C_α atoms of residues 1 and 13, exhibited a similar effect (Figure 2). Definite transitions in the end-to-end distance may be seen at 300−500 ps for peptide 2 and 700−900 ps for peptide 3 in Figure 2. The peptide 1 case is more complex. However, the time period of 2600−2800 ps may be seen as demarcating periods of significantly different behavior of the peptide length, with fluctuations over a wide range of distances (14−20 Å) at times up to 2600 ps, and subsequent relatively localized fluctuations around 15 Å. The trajectory average end-to-end distances of the peptides before the transition were 17.0, 17.2, and 18.1 Å for peptides 1, 2, and 3, respectively. The corresponding values after the transition were 15.0, 14.9, and 15.1 Å (data provided in Supporting Information). Thus, the behavior of the three peptides is qualitatively similar—their lengths decreased from 17 to 18 Å at the beginning to ca. 15 Å at the end of the simulations. The initial end-to-end distances are close to the value of 18 Å expected for the length of a 13-residue ideal α-helix, corresponding to a rise of 1.5 Å per residue (*1*, *26*). The final value of 15 Å is close to the 14.4 Å expected for the length of a 13-residue ideal π-helix, which has a rise of ca. 1.2 Å per residue (*4*, *26*).

The solvent-accessible surface areas of the simulated peptides are shown in Figure 3, with statistics provided in the Supporting Information. A decrease in the surface area may be seen to occur at about 2600−2800 ps for peptide 1, 500−700 ps for peptide 2, and 700−900 ps for peptide 3. Comparison of trajectory average values before and after the transition shows a decrease of the surface area by 98, 79, and 76 $Å^2$ for peptides 1, 2, and 3, respectively. This change is again consistent with an α to π transition; the π-helix is less elongated and is expected to have a smaller accessible

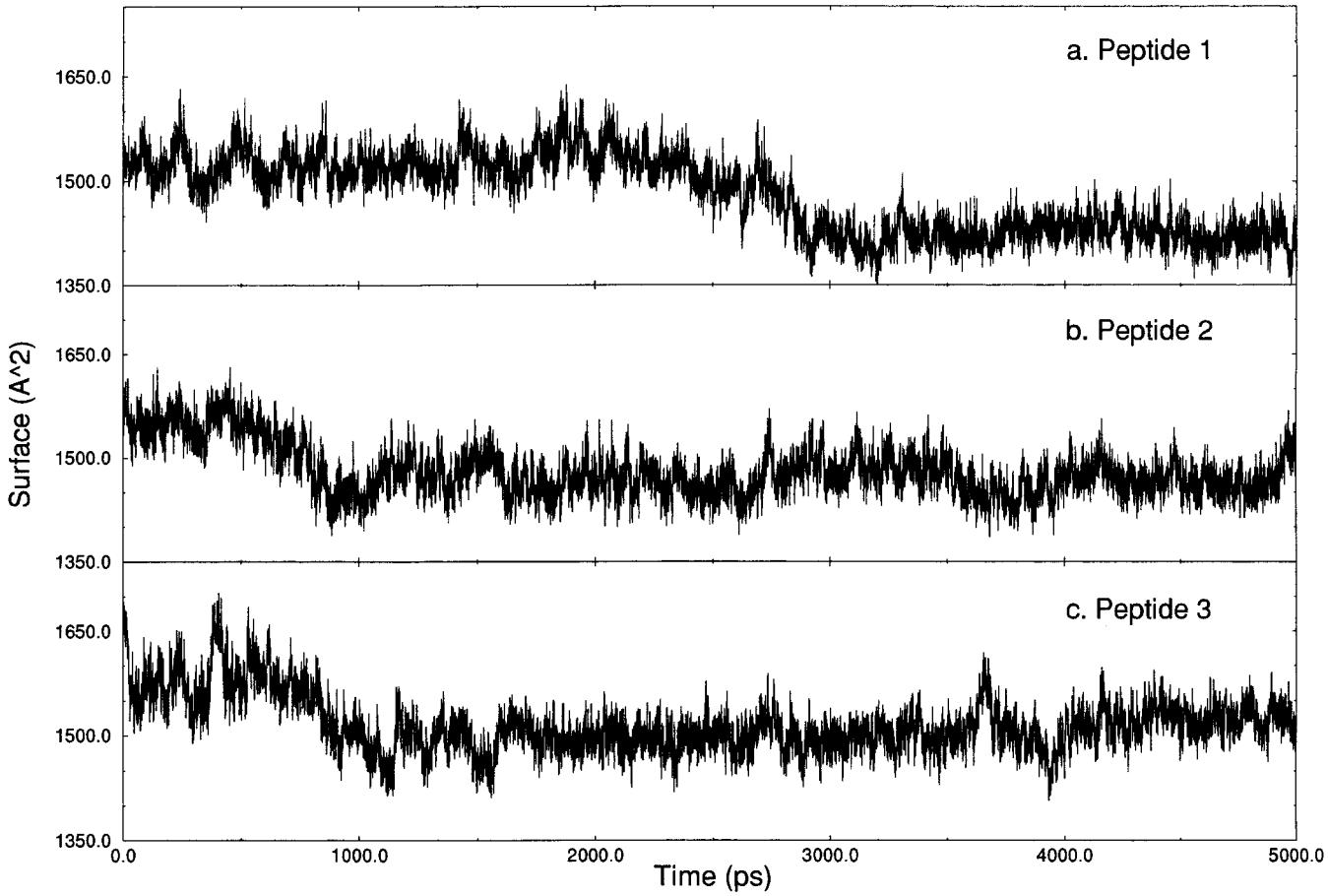

FIGURE 3: Time series of solvent-accessible surface area (in square angstroms) of (a) peptide 1 (X = A), (b) peptide 2 (X = F), and (c) peptide 3 (X = W).

Table 2: Solute−Solute Interaction Energies[a] Before and After Transitions

peptide		time (ps)	average ± SD (mean)
1	backbone−backbone	0−2800	118.4 ± 11.0 (0.7)
		2800−5000	119.0 ± 10.0 (0.7)
1	backbone−side chain	0−2800	57.6 ± 9.9 (0.7)
		2800−5000	53.9 ± 10.6 (0.7)
1	side chain−side chain	0−2800	3.6 ± 16.7 (2.5)
		2800−5000	32.5 ± 29.7 (2.5)
2	backbone−backbone	0−500	116.4 ± 8.9 (0.5)
		500−5000	119.6 ± 9.5 (0.5)
2	backbone−side chain	0−500	59.2 ± 7.9 (0.4)
		500−5000	54.3 ± 8.4 (0.4)
2	side chain−side chain	0−500	0.8 ± 12.2 (2.2)
		500−5000	4.6 ± 26.3 (2.2)
3	backbone−backbone	0−800	117.2 ± 8.7 (0.5)
		800−5000	120.0 ± 9.2 (0.5)
3	backbone−side chain	0−800	56.3± 8.5 (0.6)
		800−5000	50.9 ± 9.6 (0.6)
3	side chain−side chain	0−800	5.9 ± 13.2 (2.5)
		800−5000	2.9 ± 29.6 (2.5)

[a] Interaction energies are given in kilocalories per mole.

Table 3: Backbone−Solvent and Side Chain−Solvent Interaction Energies[a]

peptide		time (ps)	average ± SD (mean)
1	backbone−solvent	0−2800	162.6 ± 20.8 (1.4)
		2800−5000	164.5 ± 17.7 (1.4)
1	side chain−solvent	0−2800	693.6 ± 34.9 (5.2)
		2800−5000	630.3 ± 62.5 (5.2)
2	backbone−solvent	0−500	156.9 ± 14.2 (0.9)
		500−5000	165.3 ± 15.8 (0.9)
2	side chain−solvent	0−500	683.0 ± 29.6 (4.3)
		500−5000	668.6 ± 53.9 (4.3)
3	backbone−solvent	0−800	156.8 ± 15.0 (0.8)
		800−5000	164.1 ± 15.2 (0.8)
3	side chain−solvent	0−800	689.1 ± 29.9 (5.4)
		800−5000	665.2 ± 63.5 (5.4)

[a] Interaction energies are given in kilocalories per mole.

surface area than an α-helix of the same length (Mahadevan et al., unpublished results). The intramolecular and intermolecular interaction energies from the peptide simulations are shown in Tables 2 and 3; plots of the components are given in the Supporting Information. A detailed description of the energy terms is given in the Materials and Methods section. Due to large fluctuations of the energy components, it is difficult to see unambiguous indications of a structural transition in the energy plots included in the Supporting Information. However, two systematic trends may be seen in the energy averages over periods before and after the transition time, as determined from rms deviations, peptide length, and surface area. First, the average backbone−backbone energy terms increase (become less favorable) and the average backbone−solvent energy terms decrease (become more favorable) after the transition. These effects are consistent with the fact that the π-helix has one less intramolecular hydrogen bond and has more polar groups available for interactions with the solvent than does the α-helix. The second trend is the observation of less favorable side chain−solvent and more favorable side chain−backbone and side chain−side chain energy terms after the transition. This may be attributed to two effects. On one hand, the side

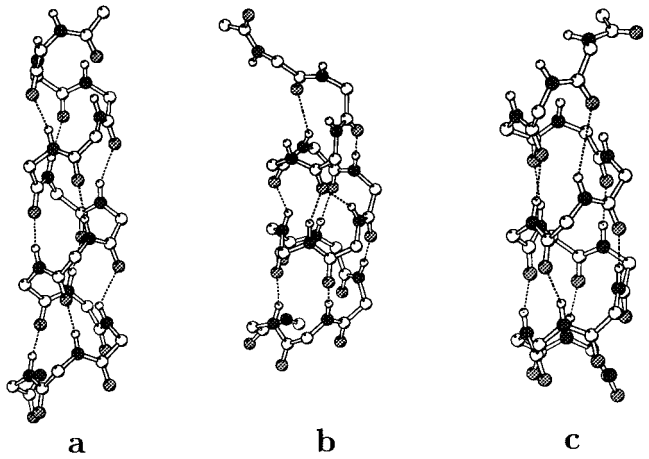

FIGURE 4: Examples of structures from peptide 1 trajectory. (a) Initial structure (α-helix); (b) at 2800 ps, transition region; (c) final structure (π-helix) Only backbone atoms are shown for clarity. Hydrogen bonds are displayed as dashed lines. C and H atoms are white; O atoms are stippled light gray; N atoms are stippled dark gray.

chains are evolving away from the arbitrarily selected, extended starting conformations, which would be expected to have highly favorable solvation and weak interactions with the backbone. On the other hand, the lowering of the side chain−side chain interaction energy appears to reflect a reorganization of the side chains into a more stable arrangement after the transition.

In conclusion, analysis of various global properties of the simulated systems consistently indicates a structural transition occurring for each of the peptides: at about 2800 ps for peptide 1, at 500 ps for peptide 2, and at 800 ps for peptide 3. Graphical inspection confirmed that peptide structures were α-helical before and π-helical after the conformational transition. Examples of structures from different stages of the peptide 1 simulation are presented in Figures 4 and 5; corresponding structures of peptide 2 and 3 are provided in the Supporting Information.

Backbone Dihedral Angle Analysis. Analysis of the time series of the peptide dihedral angles (data provided in Supporting Information) yielded further insight into the nature of the transition. The average values of backbone dihedrals calculated before and after the conformational transition tend to cluster in two different regions. For the central residues 3−9 in all three peptides, the averages over respective trajectory fragments before the transition lie in the first region, with φ between −59° and −68° and ψ between −39° and −48°. However, averages over respective trajectory fragments after the transition for residues 3−9 fall into the second region, with φ from −68° to −78° and ψ from −51° to −62°. The only exception is Ala-7 in peptide 2, which has φ and ψ values corresponding to the second region already before the transition. The first region, populated before the conformational transition in each peptide, is centered around (φ, ψ) = (−64°, −42°), which has been found as the CHARMM free energy minimum for an ideal decaalanine α-helix in water (Mahadevan et al., unpublished results) and is close to average values (−62°, −41°) found in α-helices of high-resolution protein crystal structures (*5*). The second region, populated after the transition, is centered around (φ, ψ) = (−75°, −56°), which is the free energy minimum for an ideal CHARMM π-helix in water and is close to the average geometry of π-helices in protein crystals, (φ, ψ) = (−74°, −51°), as discussed in the introduction. Thus, it is clear that the central cores of the peptides undergo a transition from an α-helical to a π-helical conformation. An additional observation is that the terminal blocking groups—acetyl at the N-terminus and amide at the C-terminus—tended to form hydrogen bonds with the peptide groups of the backbone, effectively extending the range of helical structure.

In all three peptides, backbone dihedral angles did not exhibit large conformational transitions, as seen in the relatively low fluctuations (data provided in Supporting Information). For residues 3−11 of the three peptides, φ and ψ rms fluctuations of 10−14° around the average were found. Residues 2 and 12 tended to exhibit somewhat larger fluctuations, ranging from 10° to 20° in the different simulations. The largest backbone dihedral fluctuations, as expected, were seen in the terminal residues 1 and 13, with values of about 60° found for ψ-13 in peptide 3 before the transition and for ψ-1 in peptide 3 after the transition. These large dihedral fluctuations indicate some fraying of the helices at the termini.

The detailed time evolution of the backbone dihedrals shows several interesting features. First, the terminal residues 1 and 13 (including the blocking groups), as well as residue 12, tended to explore a relatively large range of conforma-

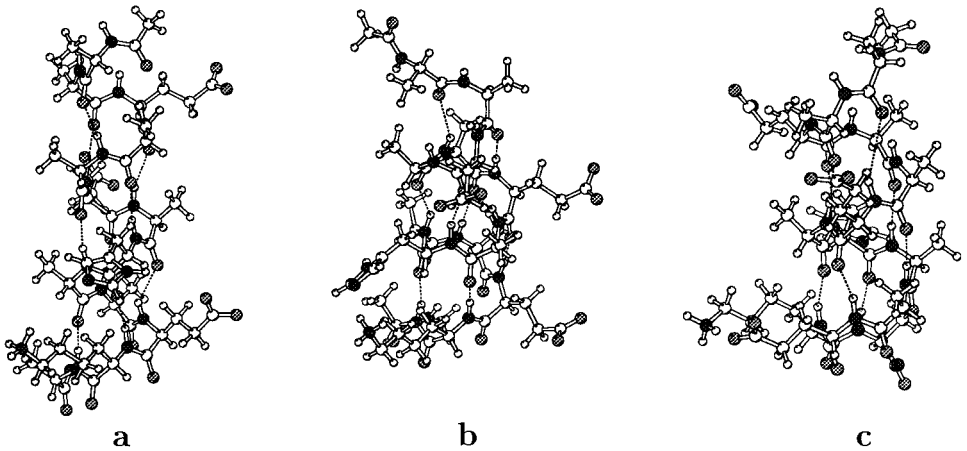

FIGURE 5: Examples of structures from peptide 1 trajectory. (a) Initial structure (α-helix); (b) at 2800 ps, transition region; (c) final structure (π-helix) All atoms are displayed. Atoms are depicted as in Figure 4.

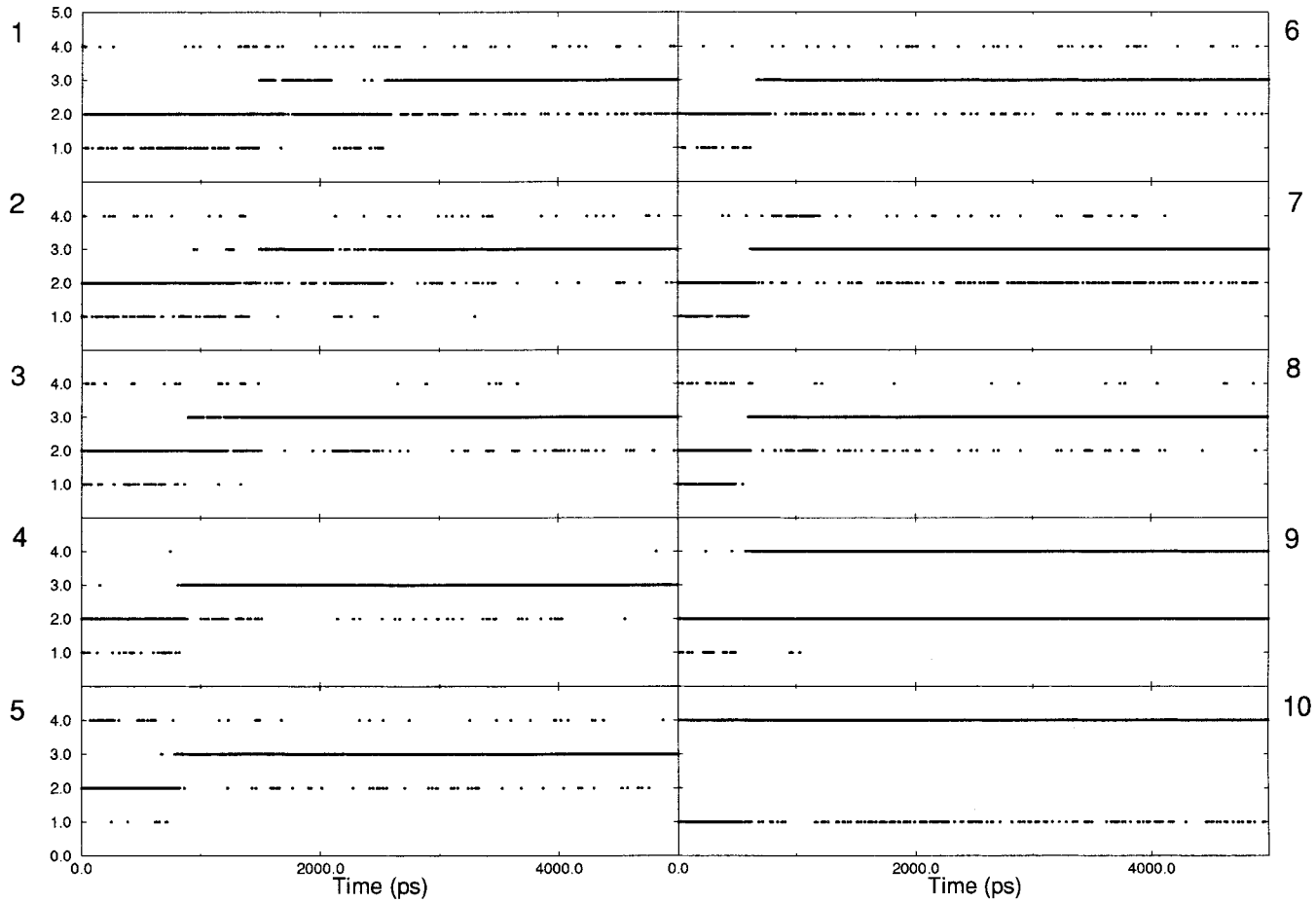

FIGURE 6: Time evolution of backbone hydrogen-bonding patterns for residues 1−10 of peptide 3. Hydrogen bond classification: 1, 3_{10}-helix ($i\cdots i+3$); 2, α-helix ($i\cdots i+4$); 3, π-helix ($i\cdots i+5$); 4, coil. See Materials and Methods for details.

tions during the whole 5 ns length of the simulations. These conformations included the three helical states considered here—the π-, α-, and 3_{10}-helices. The adoption of a π-helical conformation by the C-terminal residues appears to be the initiating event for the α to π transition in peptides 1 and 3, in which the structural change propagates systematically from the C- to the N-terminus. Thus, in peptide 1 the change from α to π occurred at 2100 ps for residue 12, at 2200 ps for residue 11−10, at 2700 ps for residues 9−6, and at 2800 for residues 5−3. In peptide 3 the structural transition took place at 500 ps for residues 11−9, at 700−800 ps for residues 8−6, at 1100 ps for residue 5, and at 1500 ps for residues 4 and 3. For peptide 2 the nature of the transition was significantly different. In this case there appeared to be two regions of initiation of the α to π transition. The central residues 5−8 underwent structural change at 300−400 ps, while residues 10 and 11 changed structure at 500 ps. This was followed by structural transitions of residue 9, at 600 ps, and residues 3−4, at 700−800 ps. Thus, from the dihedral angle standpoint, the whole structural transition took between 500 and 1000 ps to complete. From the point of view of dihedral angles, the transition in the core residues 3−8 was complete in 200 ps (peptide 1), 500 ps (peptide 2), and 800 ps (peptide 3), respectively.

Analysis of Backbone Hydrogen-Bonding Patterns. The detailed time evolution of the backbone hydrogen-bonding pattern in the peptide 3 simulation is shown in Figure 6. Analogous data for peptides 1 and 2, as well as time series of the hydrogen-bond distances, are provided in the Supporting Information. It should be noted that only residues 1−8 may form all three types of helical hydrogen bonds considered here, i.e., 3_{10}, α, and π; residue 9 may form only α and 3_{10} hydrogen bonds, and residue 10 forms only 3_{10} hydrogen bonds. Several conclusions of a general nature may be drawn from the data. First, residues 1−8 form mainly α-helical hydrogen bonds before the structural transition and mainly π-helical hydrogen bonds after the transition. (The transition times are taken to be 2800 ps for peptide 1, 500 ps for peptide 2, and 800 ps for peptide 3.) Second, throughout the simulations each of the residues 1−10 occasionally forms 3_{10}-helical hydrogen bonds; however, this is more probable at times when the predominant form is α-helix. Finally, even though residues 1−8 mostly participate in some forms of helical hydrogen bonding, in all three simulations each of these residues occasionally occupies a state without any helical hydrogen bonds—the "coil" state.

The time evolution of the hydrogen bonding pattern parallels the course of the backbone conformational change (see Backbone Dihedral Angle Analysis section). For peptides 1 and 3 the π-helical hydrogen bonds propagate from the C-terminus toward the N-terminus. Thus, in the peptide 1 simulation, the backbone hydrogen bonds change from mainly $i\cdots i+4$ to mainly $i\cdots i+5$ at about 2200 ps for residues 7 and 8 (after some minor population of $i\cdots i+5$ at 600 and 1500 ps), at 2600 ps for residues 5 and 6, and at 2700 ps for residues 3 and 4. For peptide 3 the transition is seen at 600 ps for residues 7 and 8, at 700 ps for residues 5 and 6, at 800 ps for residue 4, and at 900 ps for residue 3.

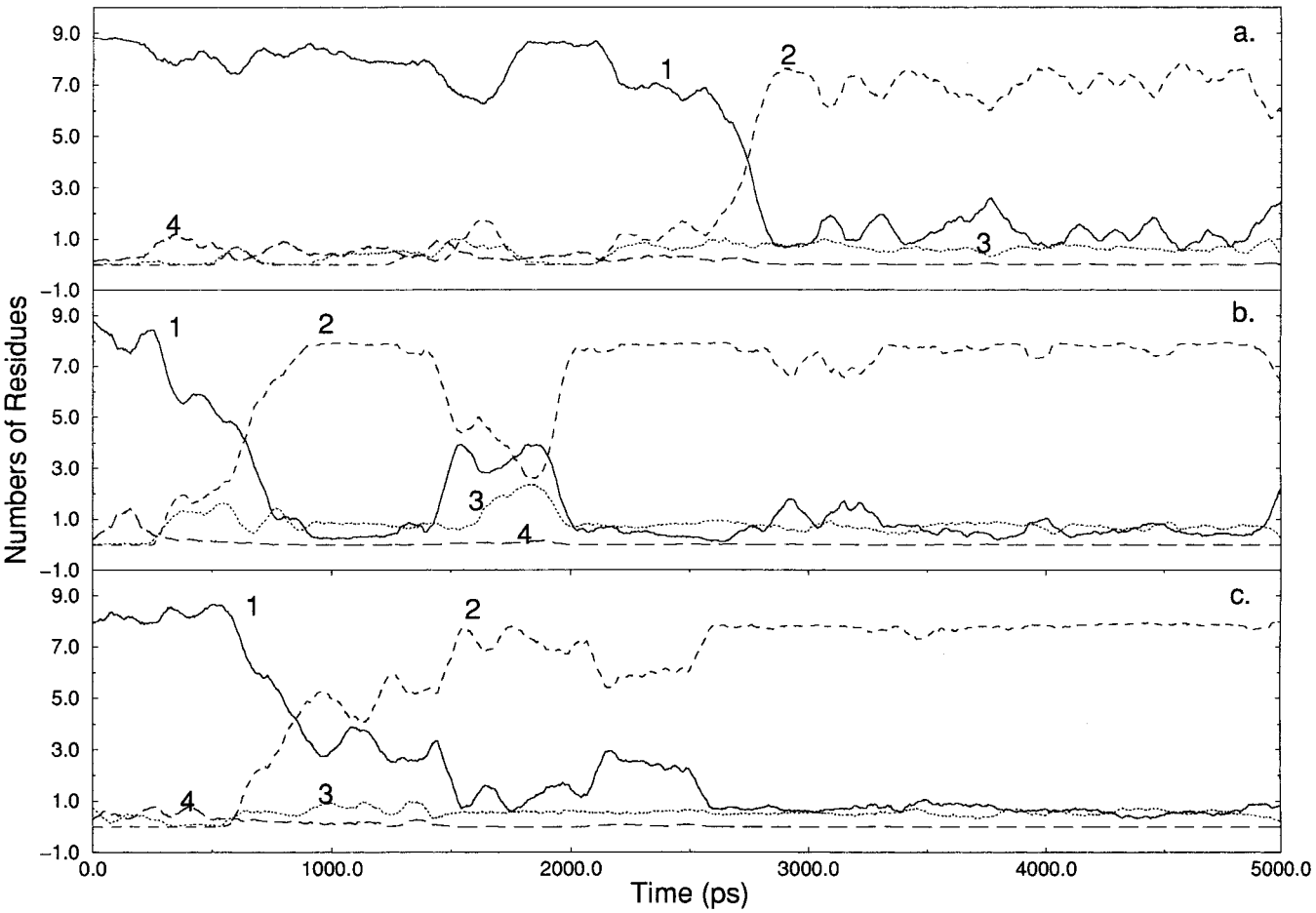

FIGURE 7: Time evolution of the total number of backbone hydrogen bonds of a given type in residues 1−10 of (a) peptide 1, (b) peptide 2, and (c) peptide 3. Hydrogen bond classification: (—, 1) α-helix; (---, 2), π-helix; (•••, 3) random coil; (— — —, 4) 3_{10}-helix. The data were smoothed with a 50 ps running average.

In the case of peptide 2, residues 4−6 undergo the α to π transition at about 300 ps, with residues 7 and 8 following at about 600 ps.

Figure 7 shows the time evolution of the total number of hydrogen bonds of a given type found in the three peptide simulations. Each of the three peptides changed from a structure with typically 6−9 α-helical hydrogen bonds at the start, to one with 6−7 π-helical and 1−2 α-helical hydrogen bonds at the end of the respective simulations. The midpoints of the transition were 2800, 600, and 800 ps for peptides 1, 2, and 3, respectively. The transitions occurred over a period of 300−500 ps. In the case of peptide 3 the hydrogen-bond reorganization was more than twice as fast as the change in backbone dihedral angles (see previous section).

Side-Chain Dynamics and Interactions. In the three 5-ns simulations of the solvated peptides, a number of side-chain dihedral angle transitions were seen. Most of these involved changes in the flexible side chain of Lys-12. Other residues exhibiting transitions were Glu-6 and His-8. Most of the side-chain dihedral transitions did not appear to be correlated with the α to π structural change in the backbone. Graphical analysis indicated that the side chains did not tend to form close intramolecular contacts but were mostly exposed to solvent. As described in the General Description of Conformational Transition section, the side chain−side chain and side chain−backbone energy terms tended to become more favorable, and the side chain−solvent energy terms less favorable, after the α to π transition (Table 2). Analysis of side chain−side chain contacts shows that for all three studied peptides a concerted rearrangement of the charged side chains occurs concurrently with the backbone structural transition. In this rearrangement the carboxylate groups of Glu-3 and Glu-6 move further apart, while the carboxylate of Glu-6 and the ammonium group of Lys-12 move closer to Glu-11. The peptides are designed to be amphiphilic, presenting a hydrophilic side to the solvent and a hydrophobic side to the heme component of the PSM complex (*27*). Our simulation results suggest that in this design the Glu-3 and Glu-6 side chains may be too close together when the peptide backbone adopts the α-helical conformation. In the isolated peptide there is no advantage of having all hydrophilic residues concentrated on one side, and the π-helical structure, with the larger Glu-3•••Glu-6 distance, becomes more stable.

Role of Water. To investigate the role of the solvent water in the α to π transitions we extracted numerous structures of the solvated peptides from the MD trajectories and performed a graphical inspection with the program QUANTA (*37*). Especially interesting were the intermediate structures sampled from the transition region. In many cases these structures involved water-mediated hydrogen bonds at the interface of the α- and π-helical regions of the peptides. We found structures in which peptide C═O groups were hydrogen-bonded to water molecules rather than to neighboring N−H groups involving residues 1, 2, 6, 7, and 8 for peptide 1, residues 3, 6, and 7 in peptide 2, and residues 1,

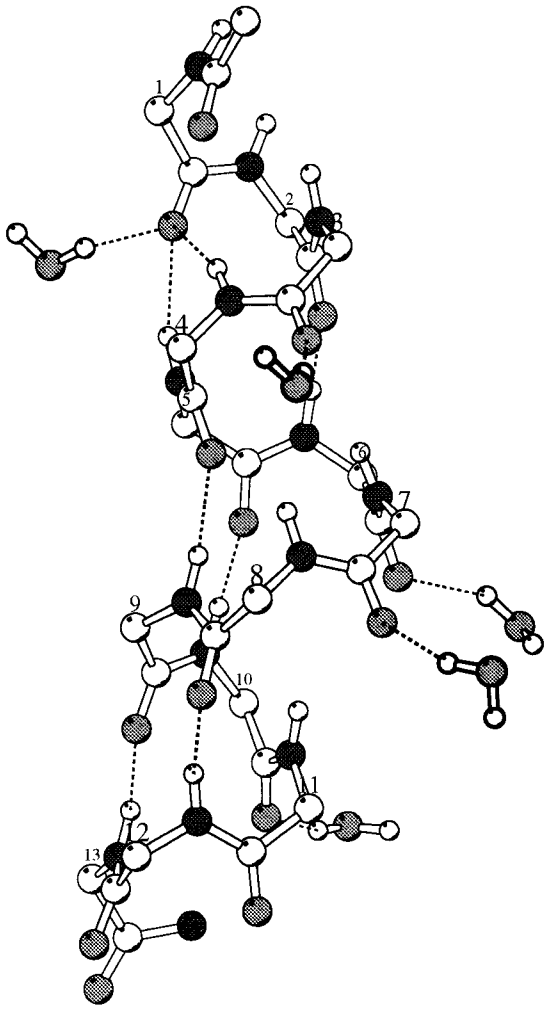

FIGURE 8: Structure at $t = 500$ ps from peptide 2 trajectory showing peptide−water interaction. Only the peptide backbone and closest waters are shown for clarity. At middle right: C═O of residues 6 and 7 interact with a water molecule each but not with N−H of residues 10, 11, or 12. At top center: C═O of residue 3 is hydrogen-bonded to a water.

2, 3, and 8 in peptide 3. Examples of water molecules disrupting backbone hydrogen-bonding patterns are given in Figure 8 and in the Supporting Information.

CONCLUSIONS

We have described molecular dynamics simulations of three 13-residue peptides exhibiting unexpected and interesting behavior. In the course of 5-ns trajectories, each of the peptides underwent a transition from a starting α-helix to a π-helical structure. The structural transition was monitored by following the time evolutions of the peptide end-to-end distances, accessible surface areas, rms deviations from starting structure, interaction energies, hydrogen-bonding patterns, and dihedral angles. The results were consistent with α → π transitions at 2800, 500, and 800 ps for peptides 1, 2, and 3, respectively. The transitions occurred sequentially and cooperatively, rather than in a concerted fashion. Structural and energetic parameters of the system corresponded to a predominantly α-helical structure before the transition and a predominantly π-helical structure after the transition. Two different transition mechanisms were seen in the simulations. For peptides 1 and 3 the transition was initiated by the adoption of a π-helical conformation in the fluctuating C-terminus and propagated from there toward the N-terminus. In the case of peptide 2 the transition was initiated in the center of the helix and propagated toward both termini simultaneously. For all three peptides the backbone structural transition was accompanied by a concerted rearrangement of the charged side chains, which included a 3 Å increase in the distance between the carboxylate groups of Glu-3 and Glu-6. Also in all three cases, the peptide backbone hydrogen-bonding patterns were disrupted at the interface between the α-helical and nascent π-helical regions, with peptide groups forming water-bridged hydrogen bonds. The time scale of the transition was between 300 and 500 ps in the three peptides, i.e., the π-helix propagation occurred at a rate of 1 residue per 50−100 ps. Although the peptide conformations were helical for most of the simulations, the structures exhibited significant fluidity. Transient unwinding occurred at the termini. Besides α- and π-helical conformations, individual residues also transiently populated the 3_{10}-helix and in a "coil" state in which peptide groups were not involved in any intramolecular hydrogen bonds.

Several of our findings are similar to effects observed in previous peptide simulations. π-Helix propagation at the rate of about one residue per 100 ps was seen in simulations of the transmembrane domain of ErbB-2 (*24*, *38*). Participation of backbone amide groups in water-bridged hydrogen bonds was seen in simulations of peptide unfolding (*39*). Transient populations of 3_{10}, π-helical, and unfolded conformers were detected in many helical peptide simulations (*23*, *39*, *40*). In some previous studies the relative stabilization of the π-helix could be attributed to favorable long-range water-mediated side chain−side chain interactions (*22*) or to destabilization of the α-helix due to high density of branched hydrophobic side chains (*24*). An analogous effect was seen in our simulations, in which the concerted reorganization of the charged side chains occurred concurrently with the backbone structural change. The side-chain rearrangements led to a net lowering of the repulsion between the three Glu carboxylate groups and increased favorable electrostatic interactions involving Lys-12.

Our results are analogous to the simulations of the sequential 3_{10} to α-helix transition of decaalanine in water (*8*). The main difference is that we report for the first time an overall transition of a whole peptide from an α-helical to a π-helical structure. Since the π-helix has been so rarely observed, it is generally believed to be less stable than the prevalent α form. In our simulations we have seen just one α → π transition for each peptide. Since no reverse transitions were seen, we can conclude that we are following an irreversible process leading from a state of higher free energy, the α-helix, to one of lower free energy, the π-helix. Thus, our simulations suggest that the π-helix is the more stable state for the three studied peptides. Because the transition occurs only once in each system, we cannot estimate the free energy difference between the two forms. After the structural transition, the peptides remain in the π-helical form for the rest of the 5 ns simulations, a period of ca. 2 ns for peptide 1, and ca. 4 ns for peptides 2 and 3. This indicates that the π-helix is at least a metastable state for these systems. Due to the finite length of the simulation, we cannot rule out the possibility that the π-helix is just an

intermediate on the way to further structural change, for example, toward complete unfolding. Experimentally, the CD spectra of the three peptides in aqueous solution at 8 °C have been interpreted as indicating a "coil" conformation, i.e., without significant secondary structure (*27*). Our results thus agree with the experimental observations in that the isolated peptides are not α-helical, while a positive experimental confirmation of the π-helical structure remains lacking. The available CD measurements indicate that the π-helices found in our simulations should be transient structures and that the peptides should eventually unfold.

The three peptides that were the object of our study are being used to construct novel hemoprotein models, the peptide-sandwiched mesohemes (*27*, *28*). The water-soluble PSMs built with the three peptides demonstrate that the His ligand coordination to the metal complexed by the porphyrin induces higher helicity of the peptides in the PSMs (*27*). We are currently working on molecular dynamics simulations of the whole PSM systems, aimed at describing their structures and fluctuations in aqueous solution. These results, as well as a comparison of the dynamics of isolated peptides with that of peptides incorporated in PSMs, will be presented in a separate paper. Especially interesting is the question whether the possibility of adoption of π-helical structures by the constituent peptides influences the properties of the PSM complexes.

While experimental evidence remains scarce, an increasing number of simulation studies are detecting the presence of the π-helical geometry in individual peptides. Using the same model as in this work, i.e., the CHARMM 22 all-atom topology and parameters (*30*), we have found that the decaalanine π-helix is much less stable than the α-helix in vacuum (*26*), while the two forms have comparable stabilities in water and DMSO solution (Mahadevan et al., unpublished results). The results of calculations with explicit solvent were confirmed by approximate solvation treatment through Poisson−Boltzmann electrostatics and a cavitation term proportional to solute surface area (Mahadevan et al., unpublished experiments). Other authors detected π-helical structures by use of various force fields—the CHARMM 19 polar hydrogen model (*22*), GROMOS (*21, 24*), and XPLOR (*24, 38*). The computational evidence thus suggests that some peptides might adopt the π-helical structure under certain conditions. Since helices are crucial structural elements of peptides and proteins, it would be highly valuable to verify these predictions on the basis of unambiguous experimental results, such as NMR spectra. Simulations with different molecular models agree on the existence of the π-helix. However, it is certain that detailed predictions such as the relative stabilities of the various helix types and the time scale and pathway for conversion between them will depend on the molecular model chosen, including the force field parameters, nonbonded cutoffs, and water model. This is clearly illustrated by the rather wide range of predictions for the relative stabilities of the α- and 3_{10}-helices in alanine and α-methylalanine peptides (*8, 9, 41*). The conditions under which the **π**-helix might exist thus require further study, including the use of approaches such as the Ewald summation (*42*) or the fast multipole method (*43*), which avoid truncating long-range electrostatic interactions known to play an important role in the structure and dynamics of biomolecules.

ACKNOWLEDGMENT

We thank the Center for Advanced Scientific Computing at the University of Kansas for use of the ORIGIN 2000 computer system. The structural figures were prepared with the program MolScript (***44*).**

SUPPORTING INFORMATION AVAILABLE

Additional tables with statistics of end-to-end distances, accessible surface areas, and backbone dihedrals and figures presenting the time evolution of interaction energies and hydrogen-bond length, as well as examples of structures sampled by peptides 2 and 3 in the trajectory. This material is available free of charge via the Internet at http://pubs.acs.org.

REFERENCES

1. Pauling, L., and Corey, R. B. (1951) *Proc. Natl. Acad. Sci. U.S.A. 37*, 235−240.
2. Donohue, J. (1953) *Proc. Natl. Acad. Sci. U.S.A. 39*, 470−478.
3. Low, B. W., and Baybutt, R. B. (1952) *J. Am. Chem. Soc. 74*, 5806−5807.
4. Creighton, T. E. (1993) *Proteins. Structures and Molecular Properties*, pp 182−188, W. H. Freeman, New York.
5. Barlow, D. J., and Thornton, J. M. (1998) *J. Mol. Biol. 201*, 601−619.
6. Baker, E. N., and Hubbard, R. E. (1984) *Prog. Biophys. Mol. Biol. 44*, 97−179.
7. Fiori, W. R., Miick, S. M., and Millhauser, G. L. (1993) *Biochemistry 32*, 11957−11962.
8. Tirado-Rives, J., Maxwell, D. S., and Jorgensen, W. L. (1993) *J. Am. Chem. Soc. 115*, 11590−11593.
9. Smythe, M. L., Huston, S. E., and Marshall, G. E. (1995) *J. Am. Chem. Soc. 117*, 5445−5452.
10. Bavioso, A., Benedetti, E., DiBlasio, B., Pavone, V., Pedone, C., Toniolo, C., and Bonora, G. M. (1986) *Proc. Natl. Acad. Sci. U.S.A. 83*, 1988−1992.
11. Toniolo, C., Crisma, M., Bonora, G. M., Benedetti, E., DiBlasio, B., Pavone, V., Pedone, C., and Santini, A. (1991) *Biopolymers 31*, 129−138.
12. Low, B. W., and Greenville-Wells, H. J. (1953) *Proc. Natl. Acad. Sci. U.S.A. 39*, 785−801.
13. Ramachandran, G., and Sasisekharan, H. (1968) *Adv. Protein Chem. 23*, 284−438.
14. Rohl, C. A., and Doig, A. J. (1996) *Protein Sci. 5*, 1687−1696.
15. Weaver, T. (2000) *Protein Sci. 9*, 201−206.
16. Weaver, T., and Banaszak, L. (1996) *Biochemistry 35*, 13955−13965.
17. Boyington, J. C., Gaffney, B. J., and Amzel, L. M. (1993) *Science 260*, 1482−1486.
18. Gaffney, B. J. (1996) *Annu. Rev. Biophys. Biomol. Struct. 25*, 431−459.
19. Sasaki, S., Yasumoto, Y., and Uematsu, I. (1981) *Macromolecules 14*, 1797−1801.
20. Musso, G. F., Patthi, S., Ryskamp, T. C., Provow, S., Kaiser, E. T., and Velicelebi, G. (1998) *Biochemistry 27*, 8174−8181.
21. Kovacs, H., Mark, A. E., Johansson, J., and van Gunsteren, W. F. (1995) *J. Mol. Biol. 247*, 808−822.
22. Shirley, W. A., and Brooks, C. L., III (1997) *Proteins: Struct., Funct., Genet. 28*, 59−71.
23. Gibbs, N., Sessions, R. B., Williams, P. B., and Dempsey, C. E. (1997) *Biophys. J. 72*, 2490−2495.
24. Duneau, J.-P., Crouzy, S., Chapron, Y., and Genest, M. (1999) *Theor. Chem. Acc. 101*, 87−91.
25. Wang, Y., and Kuczera, K. (1997) *J. Phys. Chem. B. 101*, 5205−5213.
26. Kuczera, K. (1999) in *Computational Molecular Dynamics: Challenges, Methods, Ideas* (Deuflhard, P., Hermans, J.,

Leimkuhler, B., Mark, A. E., Reich, S., and Skeel, R. D., Eds.) pp 163−175, Springer, Berlin.
27. Benson, D. R., Hart, B. R., Zhu, X., and Doughty, M. B. (1995) *J. Am. Chem. Soc. 117*, 8502−8510.
28. Liu, D., Williamson, D. A., Kennedy, M. L., Williams, T. D., Morton, M. M., and Benson, D. R. (1999) *J. Am. Chem. Soc. 121*, 11798−11812.
29. Brooks, B. R., Bruccoleri, R., Olafson, B., States, D., Swaminathan, S., and Karplus, M. (1983) *J. Comput. Chem. 4*, 187−217.
30. MacKerell, A. D., Jr., Bashford, D., Bellott, M., Dunbrack, R. L., Jr., Evanseck, J. D., Field, M. J., Fischer, S., Gao, J., Guo, H., Ha, S., Joseph-McCarthy, D., Kuchnir, L., Kuczera, K., Lau, F. T. K., Mattos, C., Michnick, S., Ngo, T., Nguyen, D. T., Prodhom, B., Reiher, W. E., III, Roux, B., Schlenkrich, M., Smith, J. C., Stote, R., Straub, J., Watanabe, M., Wiorkiewicz-Kuczera, J., and Karplus, M. (1998) *J. Phys. Chem. B 102*, 3386−3616.
31. Jorgensen, W. L., Chandrasekhar, J., Madura, J. D., Impey, R. W., and Klein, M. L. (1983) *J. Chem. Phys. 79*, 926−935.
32. Ryckaert, J. P., Ciccotti, G., and Berendsen., H. J. C. (1977) *J. Comput. Phys. 23*, 327−341.
33. Feller, S. E., Zhang, Y., Pastor, R., and Brooks, B. R. (1995) *J. Chem. Phys. 103*, 4613−4621.
34. Allen, M. P., and Tildesley, D. J. (1989) *Computer Simulations of Liquids*, Oxford University Press, Oxford, U.K.
35. Lee, B., and Richards, F. M. (1971) *J. Mol. Biol. 55*, 379−400.
36. Tidor, B., and Karplus, M. (1991) *Biochemistry 30*, 3217−3228.
37. *Quanta 98* (1998) Molecular Simulations, Inc., San Diego, CA.
38. Duneau, J.-P., Garnier, N., and Genest, M. (1997) *J. Biomol. Struct. Dyn. 15*, 555−572.
39. Tirado-Rives, J., and Jorgensen, W. L. (1991) *Biochemistry 30*, 3864−3871.
40. Duneau, J.-P., Genest, D., and Genest, M. (1996) *J. Biomol. Struct. Dyn. 13*, 753−769.
41. Zhang, L., and Hermans, J. (1994) *J. Am. Chem. Soc. 116*, 11915−11921.
42. Darden, T. A., Toukmaji, A., and Pedersen, L. G. (1997) *J. Chim. Phys. Phys.-Chim. Biol. 94*, 1346−1364.
43. Ding, H.-Q., Karasawa, N., and Goddard, W. A., III (1992) *J. Chem. Phys. 97*, 4309−4315.
44. Kraulis, P. J. (1991) *J. Appl. Crystallogr. 24*, 946−950.

BI001126B